



Cross sections for the two-step radiative decay process $X(v) \rightarrow A(v'') \rightarrow X(v')$ in e-LiH collisions

Roberto Celiberto^{1,2,a} and Annarita Laricchiuta^{2,b}

¹ Dipartimento di Ingegneria Civile, Ambientale, del Territorio, Edile e di Chimica (DICATECh) – Politecnico di Bari, Bari, Italy

² Istituto per la Scienza e Tecnologia dei Plasmi (ISTP) - Consiglio Nazionale delle Ricerche, Bari, Italy

Received 30 January 2021 / Accepted 28 April 2021 / Published online 20 May 2021
© The Author(s) 2021

Abstract. The cross sections for the two-step process, represented by the electron-impact vibro-electronic excitation $X^1\Sigma^+(v) \rightarrow A^1\Sigma^+(v'')$ of the LiH molecule, followed by radiative decay back on the vibrational manifold of the ground state, $A^1\Sigma^+(v'') \rightarrow X^1\Sigma^+(v')$, are calculated as a function of the incident electron energy from the threshold to 1000 eV. The final cross sections for the two-step process, which results in an overall vibrational excitation of the molecule, known also as *E-v process*, are provided for all the possible v, v' transitions among the vibrational levels, including the continuum, of the electronic ground state.

1 Introduction

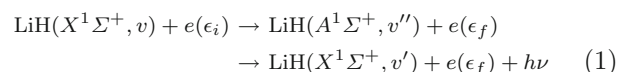
One of the main problems arising in the realization of the thermonuclear fusion for civil consumption of energy is represented by the occurrence of intense release of power flux, generated by discharge disruption and edge-localized modes [1, 2], which creates transient localized instabilities in the fusion plasma, leading to excessive thermal load on the plasma-facing components (PFC) of experimental reactors. In these conditions, in fact, the plasma-material interactions can cause serious damages to the internal device surface, resulting from the ablation, physical sputtering and chemical erosion of the wall materials. These events lead, ultimately, to adverse effects on the energy production, represented by the increase in the maintenance operations and costs of the plants, coming from the frequent wall component replacement, as well as by the reduced efficiency of the fusion reactions caused by the contamination of hydrogen plasma by the eroded materials.

Among the possible strategies to face the problem, interest has been attracted by the use of liquid metals [3, 4], which, through evaporation, can shield and protect the reactor walls, both in limiter [5–8] and divertor chambers [9–12]. Among the metallic elements (Li, Sn, Ga) used in current experimental tests in vapour shielding of PFCs [4, 12–14], lithium has proved to be one of the most promising candidates as liquid material [15] in R&D of thermonuclear fusion, due to its high evaporation rate and to its low atomic number, which allows

for a full electron stripping that prevents the radiation losses in plasma core [10], not to mention the high capability of lithium in yielding to the formation of stable hydrides which favour a low recycling of cold neutral gas [4, 9, 11, 16].

The typical mechanism that the vapour shielding is based on is originated by the conversion, through collisions, of the particle kinetic energy in internal excitation of the evaporated metallic species, followed, after relaxation, by radiation emission isotropically released in the plasma bulk, away from the walls. In this framework, lithium-containing molecules (Li₂, LiH) can play an important role. Molecular species, in fact, are characterized by several internal energy levels (rotational, vibrational and electronic) that can be collisionally excited, and after photon emission can release the extra amount of the acquired energy.

A well-known process in molecular plasma, for the conversion of collisional energy in radiation, is represented by the so-called *E-v process* consisting in a radiative decay of a molecule, following an electron-impact excitation. The *E-v* processes have been deeply investigated theoretically for H₂ molecule [17–20], because of the evidence of the contribution of this mechanism in producing a non-equilibrium vibrational distribution in negative ion sources [21, 22] and thus affecting the yield in H⁻ and the overall source efficiency. The process, involving lithium hydride, can globally be sketched as:

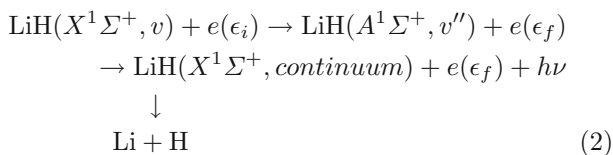


This process occurs through a first step embodying the electron collision with the LiH molecule that is initially in one of the vibrational levels belonging to the singlet

^a e-mail: roberto.celiberto@poliba.it (corresponding author)

^b e-mail: annarita.laricchiuta@cnr.it

electronic state, $X^1\Sigma^+$, and represented by the quantum number v . ϵ_i is the kinetic energy of the incident electron. The molecule is now excited to the vibrational levels, v'' , of the electronic state $A^1\Sigma^+$, also of a singlet spin-symmetry, while the incident electron gets away with the energy $\epsilon_f < \epsilon_i$. The two X and A states, owing the same molecular symmetry, are radiatively coupled, so that a decay by emission of a photon, with frequency ν and energy $h\nu$ (h is Planck's constant), can then occur. The process leads finally to an overall vibrational excitation of the ground state of the LiH molecule. The molecular excitation energy, $\Delta E_{v,v'}^X$, is given as the difference of the energy eigenvalues of the ground state vibrational levels involved in the transition, i.e. $\Delta E_{v,v'}^X = E_{v'}^X - E_v^X$. The total amount of particle energy, converted in radiation, is then given by $h\nu = (E_v^X + \epsilon_i) - (E_{v'}^X + \epsilon_f) = (\epsilon_i - \epsilon_f) - \Delta E_{v,v'}^X$. There is also the possibility that the molecule, after emission, can be left excited to the vibrational continuum of the electronic ground state; in this case, dissociation occurs with the production of Li and H atoms, according to the process:



In view of an *ab initio* modelling of the edge molecular plasma in fusion reactors, aimed to the optimization of the operative conditions for an effective vapour shielding of the PFCs, cross sections for the above (1) and (2) processes should be known. In this paper, we present a theoretical calculation of these data that, as illustrated in Sect. 2, requires, for the first step, the knowledge of the electron-impact cross sections involving the vibrationally excited LiH molecules, already available in Ref. [23], while for the second step we calculated a full set of state-specific Einstein's coefficients. Finally, in Sect. 3 the cross section results are discussed, and Conclusion of the present work is given in Sect. 4.

2 Cross section calculation

The cross section for the E - v process, coupling the vibrational levels v'' of the electronic state $A^1\Sigma^+$ with those of the ground state $X^1\Sigma^+$ of the lithium hydride, can be expressed as [17, 21, 22]:

$$\begin{aligned} \sigma_{X(v) \rightarrow A(v'') \rightarrow X(v')}(\epsilon_i) &= \sum_{v''} \sigma_{X(v) \rightarrow A(v'')}(\epsilon_i) \\ &\times \frac{A_{A(v'') \rightarrow X(v')}}{\sum_{v'} A_{A(v'') \rightarrow X(v')} + \int_{\epsilon_{th}}^{E_{max}} d\epsilon' A_{A(v'') \rightarrow X(\epsilon')}} \end{aligned} \quad (3)$$

where $\sigma_{X(v) \rightarrow A(v'')}(\epsilon_i)$ is the cross sections for the electron-impact excitation, $X(v) \rightarrow A(v'')$, of vibrationally excited LiH molecules, occurring at an incident electron energy ϵ_i . These quantities are reported in Ref. [23]. They were calculated in the *threshold modified Mott–Massey approximation*, which is derived by the well-known Mott and Massey approach to the electron scattering, but, unlike this theory which diverges at the threshold, it shows the correct vanishing behaviour. In order to validate our calculations, the obtained cross sections were compared with the results of the R -matrix method [24], which furnishes accurate values near to the process threshold (< 6 eV). Then, the calculations were extended to larger energies, typical of hot fusion plasmas (up to 1000 eV), and to all the possible vibrational excitations of the $A(v'') \rightarrow X(v')$ transition. For a deeper insight on this process and the related calculations, the reader is referred to the original paper [23]. $A_{A(v'') \rightarrow X(v')}$, is the *bound-bound* Einstein coefficient for the inverse process occurring by photon emission and ending on the v' level of the ground state. Similarly, the coefficient $A_{A(v'') \rightarrow X(\epsilon')}$ represents the *bound-free* coefficient for the decay on the ground state vibrational continuum, denoted by the continuum energy ϵ' . The integration on the denominator of Eq. (3) runs from the continuum threshold, ϵ_{th} , equal to the asymptotic energy of the potential curve of the $X^1\Sigma^+$ state [23], to the upper limit that, in principle, should be extended to infinity. In our calculation, we have imposed a cut-off, $E_{max} = 2$ eV, above the asymptote, beyond which the contribution to the integration is negligible. The *bound-bound* Einstein's coefficients $A_{A(v'') \rightarrow X(v')}(s^{-1})$ are given by [17]

$$\begin{aligned} A_{A(v'') \rightarrow X(v')} &= 2.026 \times 10^{-6} \left[\Delta E_{v'',v'}^{A,X} \right]^3 \\ &\times |\langle v'' | D(R) | v' \rangle|^2 \end{aligned} \quad (4)$$

where the transition energy $\Delta E_{v'',v'}^{A,X} = E_{v''}^A - E_{v'}^X$, expressed in cm^{-1} , is the difference between the vibrational eigenvalues of the A and X electronic states, respectively, and $D(R)$, in *a.u.*, is the transition dipole moment [23] depending on the bond length R of the molecule. These last quantities have been used also in the cross section calculation in Ref. [23] and was taken from Ref. [26]. This latter reference provides the transition dipole moments in the range of internuclear distances of 1.75–20 *a.u.* and, to the best of our knowledge, is the only calculation available in the literature. So in order to check their accuracy, we performed full CI calculation by ourselves. We found a good agreement, the largest discrepancy not exceeding 5%. Equation (4) is also valid for the *bound-free* coefficients, providing that the quantum number v' is replaced by the continuum energy ϵ' . The potential energy curves for the X and A electronic states used in the present work [25, 26], as well as the calculation of the corresponding vibrational eigenvalues and eigenfunctions, are described in Ref. [23] (see also Fig. 2).

Table 1 Comparison of the present *bound-bound* ($\sum_{v'} A_{v'',v'}$), *bound-free* ($A_{v''}$) and total ($\sum_{v'} A_{v'',v'} + A_{v''}$) Einstein's coefficients with the calculations of Partridge and Langhoff [26]. All quantities are in 10^6 s^{-1}

Present				Ref. [26]		
v''	$\sum_{v'} A_{v'',v'}$	$A_{v''}$	Total	$\sum_{v'} A_{v'',v'}$	$A_{v''}$	Total
0	41.83	0.00	41.83	36.4	0.0	36.4
1	40.48	0.00	40.48	35.2	0.0	35.2
2	39.43	0.00	39.43	34.3	0.0	34.3
3	38.60	0.00	38.60	33.6	0.0	33.6
4	37.87	0.00	37.87	32.9	0.0	32.9
5	37.20	0.00	37.20	32.3	0.0	32.3
6	36.57	0.00	36.58	31.7	0.0	31.7
7	35.96	0.04	36.00	31.1	0.0	31.2
8	35.11	0.29	35.40	30.4	0.3	30.7
9	34.28	0.60	34.87	29.0	1.3	30.3
10	32.53	1.71	34.24	27.9	2.1	30.0
11	27.67	5.93	33.60	25.3	4.4	29.7
12	25.53	8.38	33.90	20.4	8.9	29.4
13	22.83	11.75	34.58	19.6	10.0	29.6
14	21.53	14.28	35.80	19.2	10.6	29.8
15	21.59	15.32	36.91	18.6	11.8	32.9
16	19.38	19.14	38.52	18.0	12.9	32.3
17	16.80	23.91	40.72	15.7	15.4	32.1
18	16.73	25.76	42.50	15.9	16.1	31.3
19	15.72	28.69	44.41	15.6	17.9	29.9
20	14.93	31.52	46.45	12.9	22.0	28.7
21	14.23	34.79	49.02	13.4	23.6	27.1
22	14.27	36.58	50.85	11.0	27.2	26.2
23	13.54	40.03	53.57	8.6	30.6	25.6
24	12.98	43.39	56.36	7.3	33.2	24.7
25	12.30	46.56	58.86	4.5	37.2	24.0
26	7.6	51.51	59.18	2.5	40.1	23.5
27	2.7	39.48	42.19	1.2	41.9	23.2

Table 1 shows the *bound-bound* ($\sum_{v'} A_{v'',v'}$), *bound-free* ($A_{v''} = \int d\epsilon' A_{v'',\epsilon'}$) and the total sum of these two contributions of the Einstein's coefficients, compared with the calculations of Partridge and Langhoff [26]. Our calculations give results somewhat larger than those of Partridge and Langhoff. These authors, however, use their own potential curve for the ground state while we resorted to the more recent calculations by Tung et al. [25], who performed a variational approach with explicitly correlated Gaussian functions (ECGs) including adiabatic corrections, obtaining a spectroscopically accurate estimation of vibrational levels and dissociation energy. With respect to the Partridge and Langhoff calculations, this last curve presents a deeper well, inducing slightly larger transition energies which, magnified by the cube in Eq. (4), account for the differences observed in Table 1. Regarding the difference in the bound-free Einstein's coefficients, $A_{v'',\epsilon'}$, shown in the same table, it can be ascribed to the application of the Franck–Condon approximation in Ref. [26] not adopted in the present calculations.

3 Results

In this section, we present the obtained cross section data for the decay process. No experimental or theoretical data are available for comparison, so we are confident that their accuracy reflects that of the electron–molecule cross sections and Einstein's coefficients discussed in the previous section.

Figure 1 shows the cross sections for the radiative decay process (1), starting from the vibrational level $v = 0$ (Fig. 1a) and $v = 10$ (Fig. 1c) of the ground electronic state and ending on all the levels of the same state. Both plots display the cross section curves as a function of the incident electron energy, while in Figs. 1b, d the corresponding cross section maxima are shown, which give a clearer view of their dependence of on the v' levels. The vibrational behaviour of the cross sections can be qualitatively rationalized by resorting to the Franck–Condon principle (FCP) which, as is well known, is based on vertical transitions connecting the vibrational levels of different electronic states. According to the FCP, the transition probabilities, and then also the cross sections, are roughly proportional to the Franck–Condon factors (FCF) with the largest wave

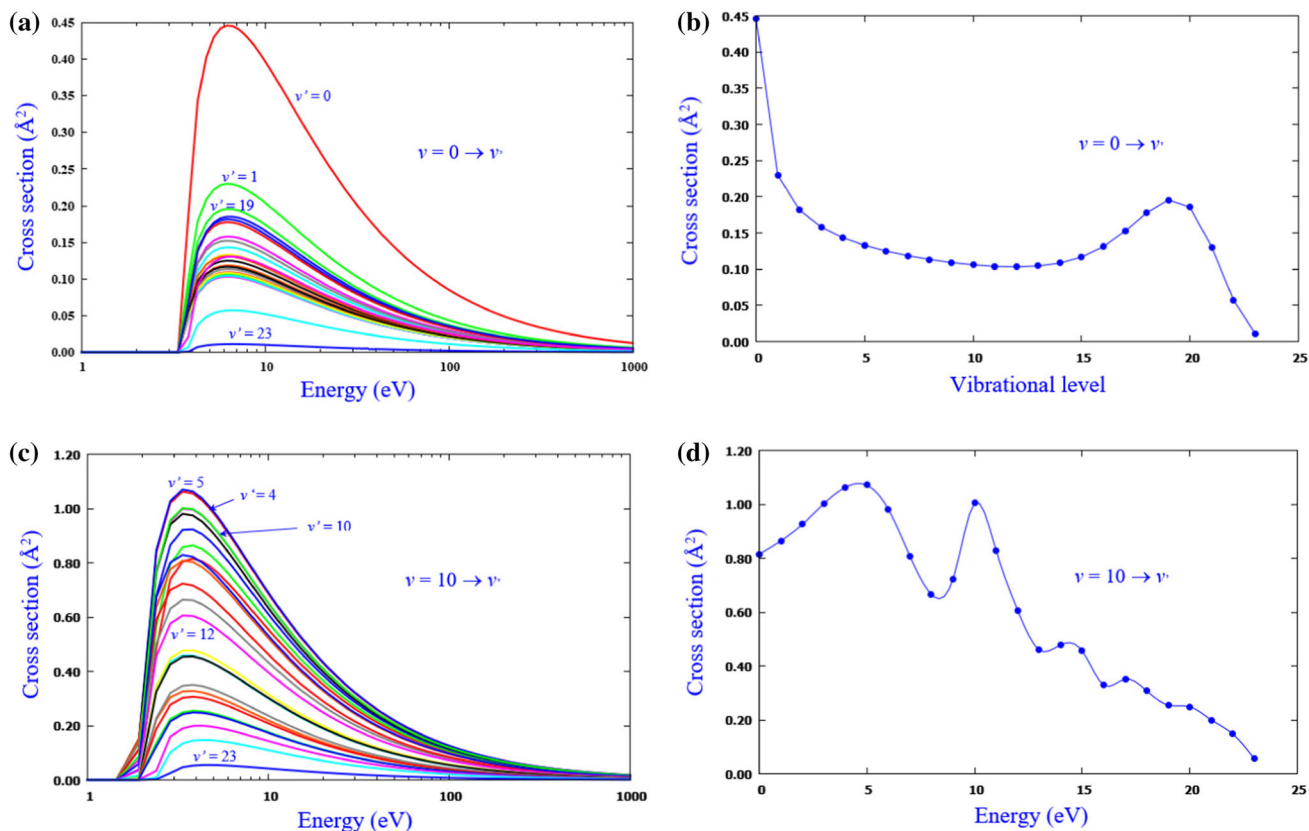


Fig. 1 **a** Cross sections as a function of electron energy for the $E-v$ process (1) starting from the level $v = 0$ and ending on all the v' levels (some indicated in the figure). **b** corresponding cross section maxima for the same process as a function of the final vibrational levels v' . Same for the lower frames but for the $E-v$ process starting from $v = 10$. In the panel (d), the cross section markers were connected by a smoothed line

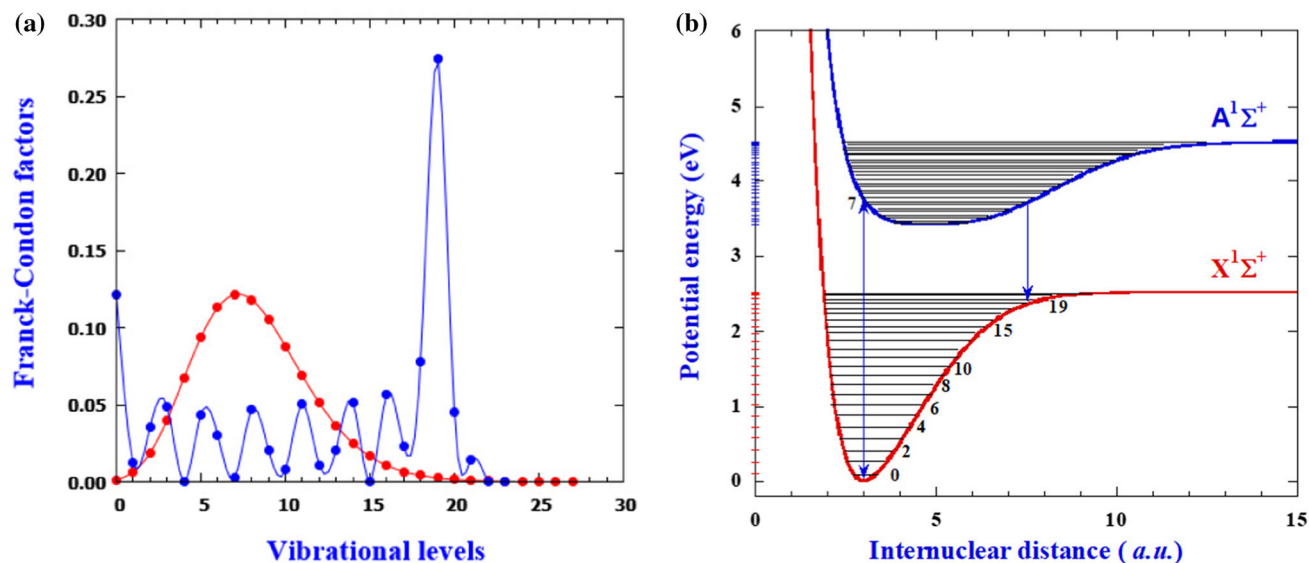


Fig. 2 **a** Franck–Condon factors for $q_{v=0,v''}$ (red) and $q_{v''=7,v'}$ (blue), for the $X(v) \rightarrow A(v'')$ and $A(v'') \rightarrow X(v')$ transitions, respectively. **b** Potential energy curves for the LiH singlet electronic states. The horizontal lines, and the corresponding ticks on the y -axis, give the energy position of the vibrational eigenvalues. In the panel (a), the markers of the FC factors were connected by a smoothed line

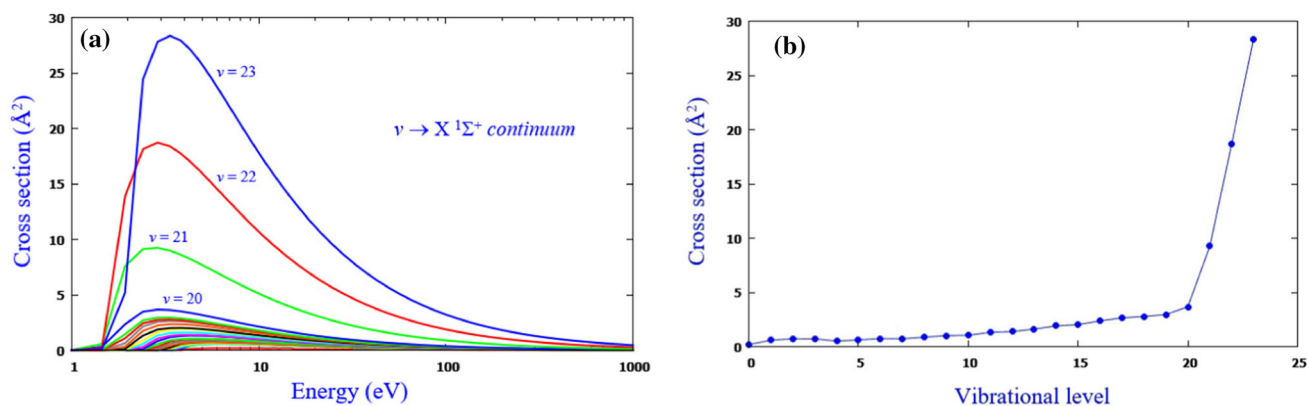


Fig. 3 **a** Cross sections as a function of the electron energy for the E - v process (2), starting from the levels $v = 0 - 23$ (some indicated in the figure) and ending on the ground state continuum. **b** Corresponding cross section maxima for the same process as a function of the initial vibrational levels v

function overlap, i.e. $q_{v,v''} = |\langle v''|v \rangle|^2$, for the electron-impact excitation, and $q_{v'',v'} = |\langle v'|v'' \rangle|^2$, for the decay relaxation. The calculated FCF are shown in Fig. 2a for both the above processes and for the case of an excitation starting from the level $v = 0$. For this level, the vertical transition originates at the equilibrium internuclear distance, where the vibrational wave function is peaked, and ends on the level $v'' = 7$ of the upper A state. The FCF, $q_{0,7}$, in fact, presents the largest value, as shown in Fig. 2a (red curve). In Fig. 2b, instead, this vertical transition is depicted by an arrow connecting the vibrational levels $v = 0$ and $v'' = 7$, belonging, respectively, to the X and A electronic states. The radiative decay also occurs following a vertical transition starting now from the level $v'' = 7$ of the A state, but at the two internuclear distances corresponding approximately to the classical turning points. As Fig. 2b shows, the final vibrational levels of the ground state, selected in the process, will then result the level $v' = 0$, as expected, and also the level $v' = 19$, since the corresponding FCF, $q_{7,19}$, is the largest for the decay, as shown in Fig. 2a (blue line). This qualitative conclusions are finally confirmed in Fig. 1b, where the largest cross section values are placed at the two final vibrational levels $v' = 0$ and $v' = 19$.

In Fig. 3a, the cross section, as a function of the energy, for the E - v process populating the vibrational continuum of the $X^1\Sigma^+$ electronic state is shown, while Fig. 3b displays the corresponding cross section maxima as a function of the initial vibrational level v . The peculiar behaviour of the cross sections in the last figure can be interpreted again at the light of the FCP. The vertical transition, starting from the level v , will select the level \bar{v}'' with the largest FC factor, $q_{v,\bar{v}''}$, whence the decay on the ground state continuum will occur, governed by the Einstein's coefficient $A_{\bar{v}''}$. Both the $q_{v,\bar{v}''}$ and $A_{\bar{v}''}$ are reported in Table 2, while Fig. 4 shows the Einstein coefficients as a function of the starting vibrational levels. The curve reproduces quite well the cross section behaviour of Fig. 3b. It is worth noting that the considerations made about the behaviour

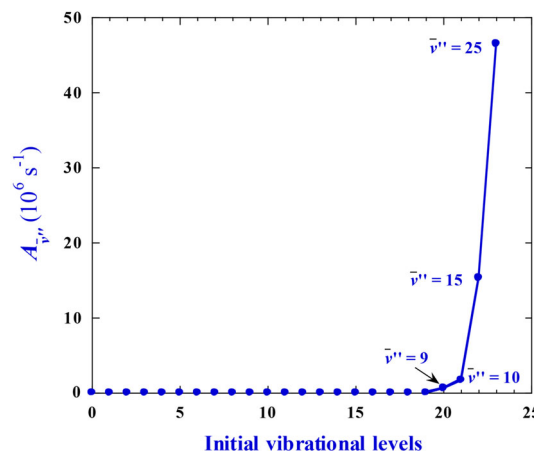


Fig. 4 Einstein's coefficients $A_{\bar{v}''}$ as a function of the starting levels v for the two-step transitions $v \rightarrow \bar{v}'' \rightarrow v'$, where \bar{v}'' denotes the level of the electronic state $A^1\Sigma^+$ reached by a vertical excitation. In the figure are shown also the values of \bar{v}'' for the last four points (see Table 2)

of the dissociative radiative decay cross sections with the initial vibrational quantum number are quite general; in fact, as shown in Ref. [17–19], also in the case of E - v involving the singlet states of H_2 the dissociative channel becomes the dominant one for the highest vibrational levels, characterized by large positive interference with the continuum wavefunctions.

4 Conclusion

In this work, we presented the cross sections for the so-called E - v process, occurring in lithium hydride through two steps, i.e. the vibro-electronic excitation of the molecule by electron impact, from the ground vibrational levels to those of the first excited electronic state, followed by a radiative decay, by photon emission, back to the initial state. The cross sections were obtained as

Table 2 FC factors, $q_{v,\bar{v}''}$, and Einstein coefficients, $A_{\bar{v}''}$, for each initial vibrational level v . The second column shows the vibrational level \bar{v}'' of the upper electronic state, involved in a vertical transition from the level v and therefore with the largest FC factor. ($1.23(-01) \equiv 1.23 \cdot 10^{-01}$)

v	\bar{v}''	$q_{v,\bar{v}''}$	$A_{\bar{v}''} (10^6 s^{-1})$
0	7	0.121	4.00(-02)
1	4	0.104	6.71(-09)
2	2	0.103	8.53(-07)
3	1	0.104	1.71(-05)
4	1	0.112	1.71(-05)
5	0	0.115	6.71(-09)
6	0	0.141	6.71(-09)
7	0	0.150	6.71(-09)
8	0	0.141	6.71(-09)
9	0	0.116	6.71(-09)
10	1	0.106	1.71(-05)
11	1	0.131	1.71(-05)
12	1	0.119	1.71(-05)
13	2	0.133	8.53(-07)
14	2	0.127	8.53(-07)
15	3	0.152	1.71(-05)
16	4	0.167	2.88(-04)
17	5	0.189	1.91(-03)
18	6	0.229	4.70(-03)
19	7	0.274	4.07(-02)
20	9	0.311	5.99(-01)
21	10	0.306	1.71
22	15	0.164	15.3
23	25	0.162	46.6

a function of the incident electron energy and for all the involved initial and final vibrational levels of the ground state. We have also shown that the whole E - v process is governed, according to the FCP, by vertical transitions in both the two steps. These results can be used as input data in the modelling of molecular plasmas, aimed to the simulations of the vapour shielding techniques studied in thermonuclear fusion [14]; the complete datasets will be available through the Phys4EntryDB (<http://phys4entrydb.ba.imip.cnr.it/Phys4EntryDB/>).

Acknowledgements The support of this work by the International Atomic Energy Agency (through RA No. 23255/R0 with RC) is gratefully acknowledged. We would like to devote the present paper to the memory of the late Prof. Ratko K Janev, who originally inspired the work.

Funding Open access funding provided by Politecnico di Bari within the CRUI-CARE Agreement.

Data Availability Statement This manuscript has associated data in a data repository. [Authors' comment: The data set generated in this work will be made available at the URL <http://phys4entrydb.ba.imip.cnr.it/Phys4EntryDB/>.]

Open Access This article is licensed under a Creative Commons Attribution 4.0 International License, which permits use, sharing, adaptation, distribution and reproduction in

any medium or format, as long as you give appropriate credit to the original author(s) and the source, provide a link to the Creative Commons licence, and indicate if changes were made. The images or other third party material in this article are included in the article's Creative Commons licence, unless indicated otherwise in a credit line to the material. If material is not included in the article's Creative Commons licence and your intended use is not permitted by statutory regulation or exceeds the permitted use, you will need to obtain permission directly from the copyright holder. To view a copy of this licence, visit <http://creativecommons.org/licenses/by/4.0/>.

References

1. A.H. Boozer, Phys. Plasmas **19**, 058101 (2012)
2. W. Suttrop, Plasma Phys. Control. Fusion **42**, A1–A14 (2000)
3. F.L. Tabares, Plasma Phys. Control. Fusion **58**, 014014 (2016)
4. R.E. Nygren, F.L. Tabares, Nucl. Mater. Energy **9**, 6 (2016)
5. R. Majeski et al., J. Nucl. Mater. **625**, 313 (2003)
6. M.L. Apicella et al., J. Nucl. Mater. **363–365**, 1346 (2007)
7. R.B. Gomes et al., J. Nucl. Mater. **415**, S989 (2011)
8. V.A. Evtikhin et al., Plasma Phys. Control. Fusion **44**, 955 (2002)
9. R. Kaita et al., Phys. Plasmas **14**, 056111 (2007)
10. D.G. Whyte et al., Fusion Eng. Des. **72**, 133 (2004)
11. H.W. Kugel et al., Fusion Eng. Des. **87**, 1724 (2012)
12. M.A. Jaworski et al., Nucl. Fusion **53**, 083032 (2013)
13. G.G. van Eden, V. Kvon, M.C.M. van de Sanden, T.W. Morgan, Nature Commun. **8**, 192 (2017)
14. *Atomic Data for Vapour Shielding in Fusion Devices*, Summary Report of the First Research Coordination Meeting, IAEA Headquarters, Vienna, Austria, 13–15 March 2019 (<https://www.nds.iaea.org/publications/indc/indc-nds-0781>)
15. F.L. Tabares, Y. Hirooka, R. Maingi, G. Mazzitelli, V. Mirnov, R. Nygren, M. Ono, D.N. Ruzic, Conf. Rep. Nucl. Fusion **56**, 127002 (2016)
16. M.J. Baldwin, R.P. Doerner, S.C. Luckhardt, R.W. Conn, Nucl. Fusion **42**, 1318 (2002)
17. R. Celiberto, M. Capitelli, U.T. Lamanna, Chem. Phys. **183**, 101 (1994)
18. R. Celiberto, M. Capitelli, A. Laricchiuta, Phys. Scr. **T96**, 32 (2002)
19. A. Laricchiuta, R. Celiberto, F. Esposito, M. Capitelli, Plasma Sources Sci. Technol. **15**, S62–S66 (2006)
20. L.H. Scarlett, J.K. Tapley, J.S. Savage, D.V. Fursa, M.C. Zammit, I. Bray, Plasma Sources Sci. Technol. **28**, 025004 (2019)
21. J.R. Hiskes, J. Appl. Phys. **51**, 4592 (1980)
22. J.R. Hiskes, J. Appl. Phys. **70**, 3409 (1991)
23. R. Celiberto, R.K. Janev, A. Laricchiuta, Plasma Sources Sci. Technol. **29**, 035008 (2020)
24. B.K. Antony, K.N. Joshipura, N.J. Mason, J. Tennyson, J. Phys. B: At. Mol. Opt. Phys. **37**, 1689–97 (2004)
25. W.C. Tung, M. Pavanello, L. Adamowicz, J. Chem. Phys. **134**, 064117 (2011)
26. H. Partridge, S.R. Langhoff, J. Chem. Phys. **74**, 2361 (1981)